

A tunable Shack-Hartmann wavefront sensor based on a liquid-filled microlens array

This article has been downloaded from IOPscience. Please scroll down to see the full text article.

2008 J. Micromech. Microeng. 18 105017

(<http://iopscience.iop.org/0960-1317/18/10/105017>)

[The Table of Contents](#) and [more related content](#) is available

Download details:

IP Address: 137.132.123.74

The article was downloaded on 03/10/2008 at 02:45

Please note that [terms and conditions apply](#).

A tunable Shack–Hartmann wavefront sensor based on a liquid-filled microlens array

Yu Hongbin, Zhou Guangya, Chau Fook Siong, Lee Feiwen and Wang Shouhua

Micro/Nano Systems Initiative Technology, Department of Mechanical Engineering, National University of Singapore, 117576, Singapore

E-mail: mpezgy@nus.edu.sg

Received 16 June 2008, in final form 24 July 2008

Published 12 September 2008

Online at stacks.iop.org/JMM/18/105017

Abstract

A novel design concept for a Shack–Hartmann sensor is presented. A liquid-filled microlens array is used to replace the commonly used microlens array with fixed focal length in a conventional type. The focal length tunability associated with this design can provide the device with the advantage that its performance can be flexibly chosen between a large dynamic range and a high sensitivity preferred region. At the same time, it is also possible to possess both of these characteristics simultaneously with a particular procedure. This feature allows the device to be operated in different applications. The results of a prototype demonstrated in this paper qualitatively verify this feasibility, and the potential application perspective of this design is also presented.

(Some figures in this article are in colour only in the electronic version)

1. Introduction

A wavefront sensor is an instrument used to measure the transmittance wavefront of an optical beam and can be adopted to evaluate the quality of a laser beam and optical components as well as measuring the optical aberration induced by environment [1]. With the advent and development of adaptive optical technology, the significance of a wavefront sensor becomes more and more distinct, since it can provide information about the variation of a working condition in real time to the controller so as to actuate the corrector to perform active action accordingly. To date, it has been widely used in various applications such as a high power laser or laser shaping systems [2], astronomical observation telescopes [3] and ophthalmic-analysis systems [4]. There are numerous approaches to measure the wavefront, among which the Shack–Hartmann method has been proven as the most practical and robust techniques [5, 6]. A Shack–Hartmann-type wavefront sensor consists of a microlens array and a charge-coupled device (CCD) [7], in which the microlens array is used to dissect the incoming wavefront into a number of segments and each microlens in the array creates a focal

spot within the assigned subaperture on the CCD. When any variation is introduced into the beam wavefront, the positions of the spots on the CCD will change accordingly as shown in figure 1. By measuring the lateral displacement of the spots with respect to the reference position of a plane wave, the average wavefront slope over each microlens aperture can be determined, with which the wavefront can be finally expressed as a series of Zernike polynomials [8, 9].

With respect to the working principle, it is obvious that the measurement of the spots' lateral displacement is a critical step for this type of wavefront sensor. At the same time, this displacement is directly determined by the focal length of microlens as well as the wavefront. With a constant lenslet size, longer focal length can provide higher sensitivity but shows a smaller measurement dynamic range, while shorter focal length can increase the dynamic range but at the expense of reducing sensitivity. In a conventional Shack–Hartmann wavefront sensor, however, the microlens usually has fixed focal length. As a result, in this case, the focal length has to be selected by considering the tradeoff between the dynamic range and sensitivity. This will definitely limit the application of this type of wavefront sensor. A few

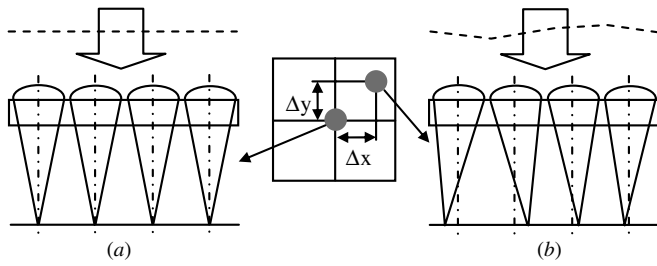


Figure 1. Schematics of the Shack–Hartmann wavefront sensor. (a) Plane wavefront, (b) aberrated wavefront.

methods have been proposed to overcome this problem. Some researchers focused on the solutions from software treatment [10–12], while others tried to improve the performance of the wavefront sensor from the hardware aspect (the same as our solution presented below). Seifert *et al* [13] adopted a dynamic liquid crystal display (LCD) to replace the static microlens array, in which the LCD was used to display an array of Fresnel microlenses. Thereby, the microlens parameters such as focal length, aperture size and position can be changed to adapt to the wavefront. Choo and Muller used an addressable microlens array to improve the dynamic range, in which the microlenses with constant focal length in the array can be individually actuated to mechanically resonate so as to identify their corresponding focal spots on the CCD [14]. As a result, the dynamic range can be improved significantly. While in the method proposed by Yoon *et al* [15], the key to the expanding dynamic range is the use of a translatable plate blocking adjacent lenslet that increases the spacing between wavefront sensing spots.

In this paper, a relatively simple way based on optofluidic technology is presented. A tunable liquid-filled microlens array integrated with a microfluidic network is adopted to replace the aforementioned microlens array with fixed focal length. As shown in figure 2, by dynamically adjusting the focal length of the microlens, the Shack–Hartmann wavefront sensor can be flexibly selected to work between a large dynamic measurement range (shorter focal length status) and a high sensitivity (longer focal length region) preferred region, or possessing both of them simultaneously by using a particular operation procedure. For example, when using in an adaptive optical (AO) system, the shorter focal length can be used first to capture the large wavefront distortion. After being compensated coarsely by a corrector (deformable mirror), the microlens can be then tuned into a longer focal length status for further fine correction. With this working route, the improved performance of the AO system, including a large dynamic range together with high correction precision, can be obviously foreseen. At the same time, the relatively simple fabrication process and the capability of massive production with low cost associated with the liquid microlens array also make it an attractive candidate over the conventional one.

2. Design and fabrication

As mentioned above, the most commonly used microlens array with fixed focal length must undoubtedly seek a compromise

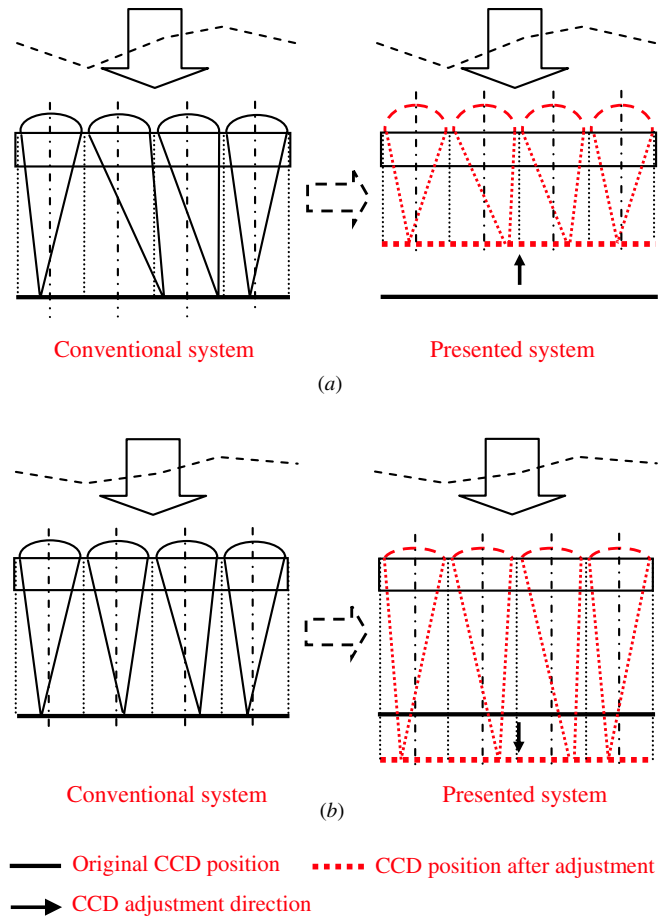


Figure 2. Schematics of design working theory. (a) Large dynamic measurement range. In some cases, the lateral shift of focal spots may exceed the subaperture region making it difficult to distinguish individual focal spots with respect to their subaperture, therefore causing problems to the wavefront reconstruction. By tuning the microlens to the shorter focal length status, all of the spots' lateral shift will be reduced. As a result, all the spots will fall into their corresponding subaperture area again and the wavefront can then be successfully reconstructed. (b) High sensitivity. With respect to a small aberrated wavefront, the resultant spots' lateral shift is very small, thereby increasing the potential error in quantitative determination of the shift amount or even overlooking this small variation. By adjusting the microlens to a longer focal length status, all of the small shift will be magnified simultaneously. This phenomenon, namely small aberration, can cause a large spot shift, which means high sensitivity. (The grey (red online) color refers to the situation where the liquid microlens array is used while the black color corresponds to the case of a solid microlens array with fixed focal length, and all of the statements mentioned above are based on a comparison with this case. Meanwhile, the black dotted lines between the microlens array and the CCD are used to assign the corresponding subaperture area on the CCD to the individual microlens.)

between the dynamic measurement range and the measurement sensitivity for the device performance. Recently, a novel type of a microlens array, namely a liquid microlens array, has obtained more research interest mainly for dynamic imaging applications [16–20] due to its focal length tunability and the relatively easy and low cost fabrication. This type of microlens is derived from the technology initially developed in the lab-on-a-chip area and usually consists of a deformable elastic

membrane, hollow cavity and microchannel as described in [16–20]. The top of the hollow cavity fabricated into a transparent substrate is covered by an elastic membrane, constituting a closed space. The fluid (working medium of the liquid lens) is introduced into this space via the microchannel using a pressure-driven method. With the increased hydraulic pressure, the membrane will be forced to deform into a spherical-like shape with the sag height δ given by

$$\delta = 3Pa^4 \times (1 - \nu^2)/(16Eh^3). \quad (1)$$

As a result, the liquid sealed into the closed cavity will build a lens structure with particular focal length f :

$$f = R/(n - 1), \quad (2)$$

where a and h are the radius and thickness of membrane, respectively. E and ν correspond to Young’s modulus and Poisson’s ratio of membrane material (for PDMS, $E = 3$ MPa, $\nu = 0.49$). P is the applied pressure and n is the refractive index of the filled fluid, while R is the radius of curvature of membrane, which is relevant to δ and a .

The pressure-controlled membrane deformation, namely the radius of curvature of liquid lens, provides the lens with the tunability for focal length. It is obvious that when the liquid-filled microlens array is used to replace the microlens array with fixed focal length in the Shack–Hartmann wavefront sensor, the problem as mentioned above can be readily solved by this particular characteristic, in which the short focal length status can be utilized to provide the large dynamic measurement range while the high sensitivity performance can be realized by using the long focal length on the same device. To the best of our knowledge, it is the first time that the application of the liquid microlens array is extended into the wavefront sensing region. Meanwhile, it can be foreseen that some applications especially for adaptive optics will benefit more from the combination of these two technologies.

Since the key idea of our design is the focal length tunability provided by liquid-filled microlens, the main task during the design step is to determine the dimensional parameters for the lens structure, in which both mechanical and optical aspects should be considered. Figure 3 shows the schematic of the design flow. First, the number and the diameter of microlens in the array are preliminarily determined with respect to the size of the CCD-sensitive area and the fabrication rule. Then a value is pre-assigned to the membrane thickness. Through mechanical analysis, the deflection range as well as the tunable range of the focal length under a steady working condition (the maximum applied pressure is limited by the bonding strength at the interface between the membrane and the chamber substrate) can be derived. If this cannot cover the desired focal length tunable range, a small reduction to the thickness is performed followed by repeating the same procedure as mentioned above until the design requirement is finally met. The structural parameters of the microlens adopted in our design are listed in table 1.

Like most of the devices based on optofluidic technology [21–23], the microlens array in our design is also made from polydimethylsiloxane (PDMS) due to its good optical transmission property in a wide spectrum range (from near ultraviolet to near infrared) and excellent mechanical property

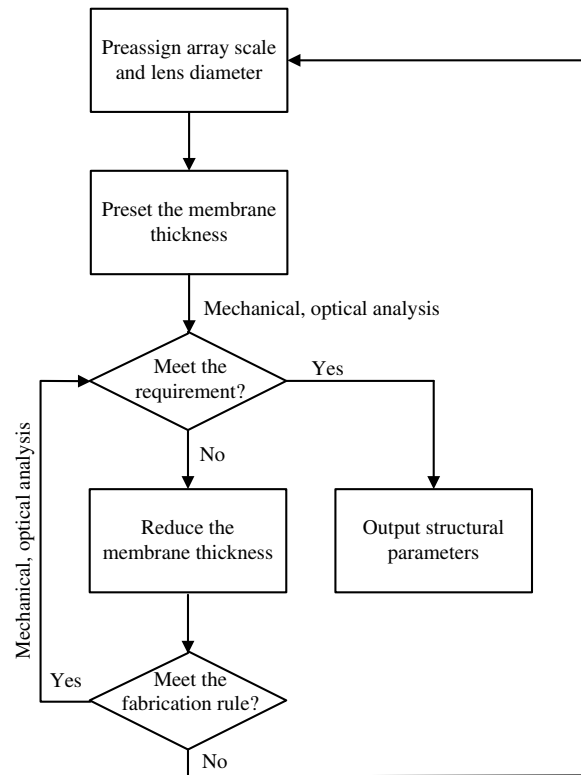


Figure 3. Design flow.

Table 1. Structural dimensions of the design.

Part	Design parameter
Liquid microlens array	6 × 5
Microlens diameter	400 μm
Membrane thickness	30 μm
Microchannel width	50 μm

as elastic material. Soft lithography and oxygen plasma activated bonding are the two main technologies involved in the fabrication process. Hence, the device fabrication process is greatly simplified and it is possible for mass production with low cost. The specific process flow is shown in figure 4. One SU-8 layer of 100 μm thickness was first spun onto a 4 inches polished silicon wafer. After performing the standard photolithography procedure, the cavity and microchannel for the lens structure were simultaneously patterned into this SU-8 layer (figure 4(a)) acting as the master mold for the subsequent PDMS casting process as shown in figure 4(b), in which a liquid PDMS prepolymer (Sylgard 184 silicone elastomer, a base and curing agent of Dow Coming Corp., mixed in a 10:1 weight ratio) was evenly poured onto the mold to form a 3 mm thick layer. After curing under 60 °C for 2 h, this PDMS substrate with the pattern having been transferred was peeled off from the mold (figure 4(c)). A PDMS membrane with 30 μm thickness was spun onto another polished silicon wafer followed by thorough curing (figure 4(d)). These two parts were then bonded together under the assistance of oxygen plasma, as shown in figure 4(e). Finally, holes were manually drilled at both ends of the microchannel, through which the liquid can be introduced with an external syringe pumping

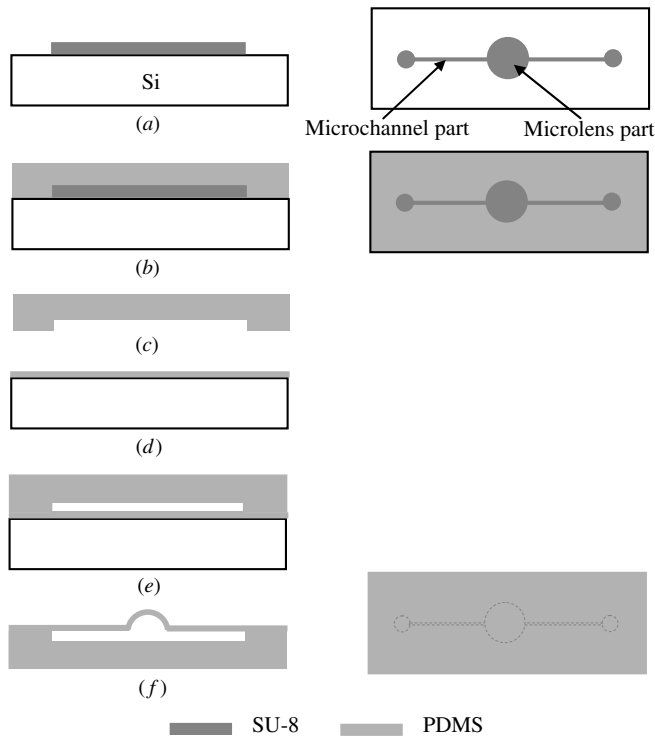


Figure 4. Fabrication process of a liquid microlens array.

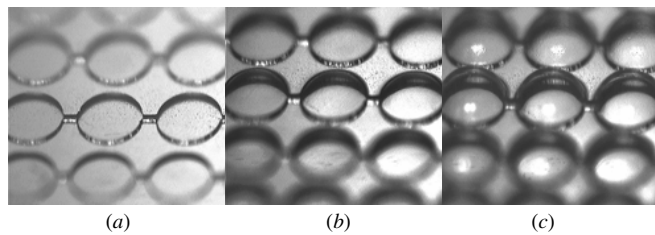


Figure 5. Pictures of the fabricated microlens array under different applied pressures. (a) 0 kPa, focal length: ∞ ; (b) 2 kPa, focal length: 12.68 mm; (c) 6 kPa, focal length: 4.95 mm.

system (figure 4(e)). Figure 5 shows the fabricated microlens array under different working pressures, namely 0 kPa, 2 kPa and 4 kPa.

3. Experiment results

3.1. Liquid microlens array

Figure 6(a) shows a picture of the fabricated 6×5 liquid microlens array in one working status, and one microlens in the array is selected to demonstrate the cross-section contours along both the horizontal and the vertical directions (figure 6(b)), which are measured with a ZYGO non-contact optical profiler. Through data analysis, the RMS and peak-to-valley (PV) difference between these two contours are calculated to be 76 nm and 125 nm, respectively, while the microlens diameter and its sag height are measured to be $399.801 \mu\text{m}$ and $19.485 \mu\text{m}$. At the same time, in order to test the uniformity between microlenses in the array, the cross-section contours of all of the microlenses in the array

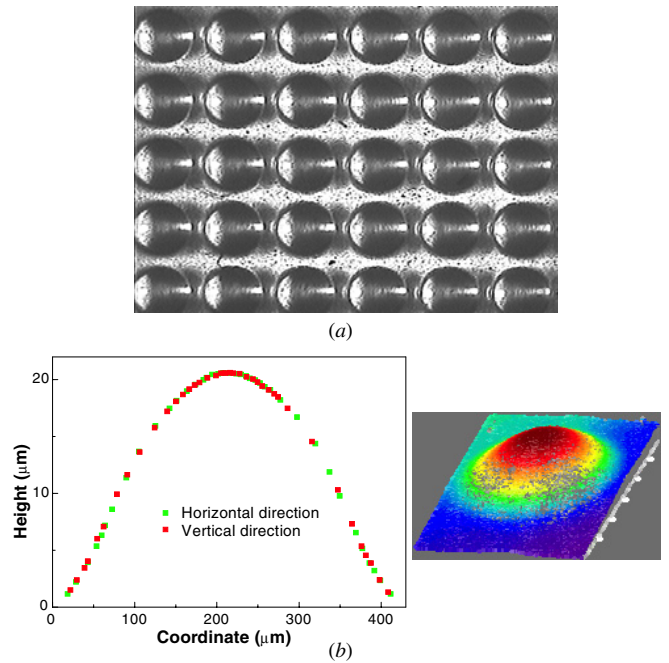


Figure 6. Picture of the fabricated microlens array. (a) Microscopy picture of the fabricated microlens array and (b) ZYGO profiler measurement. Left: the cross-section profile of one microlens; right: 3D profile of the microlens. (Before measuring with the ZYGO profiler, a thin layer of gold must be deposited onto the device to provide the required reflective surface because PDMS is transparent. At the same time, since PDMS is a pliable material, the surface quality of the gold layer is not very good. Therefore, the demonstrated 3D profile is a bit rough, unlike the real situation.)

under the same working conditions are recorded as well. After performing statistic analysis, the standard deviation of the microlens profile is deduced to be 135 nm. Meanwhile, the average microlens diameter is $399.953 \mu\text{m}$ with a standard deviation of 89 nm, while the average sag height is $19.552 \mu\text{m}$ with a standard deviation of 118 nm.

Considering the fact that the focal length tunability is the most interested feature of the microlens for the Shack–Hartmann wavefront sensor application, the individual value of the focal length of one microlens in the array under different applied pressures is recorded and shown in figure 7 together with the error bar obtained between five measurements. The specific measurement method for the focal length of the liquid microlens is the same as that shown in [24].

From the results, it can be seen that the focal length of our fabricated liquid microlens can be tuned from tens of millimeters to nearly 2 mm in the whole operation range with good repeatability between multiple tests. Meanwhile, the uniformity between different microlenses in the array is also proved to be very well. Combining the considerations about the optical aspect and operation, the longest and shortest focal lengths of the microlens are chosen to be 25.58 mm (1 kPa) and 7.88 mm (3.25 kPa), respectively, for the following demonstration experiment. From theoretical analysis, the dynamic measurement range of the Shack–Hartmann sensor when equipped with 7.88 mm focal length is about 3.25 (25.58/7.88) times larger than the case of 25.6 mm, while with respect to the sensitivity, the situation is totally inverse.

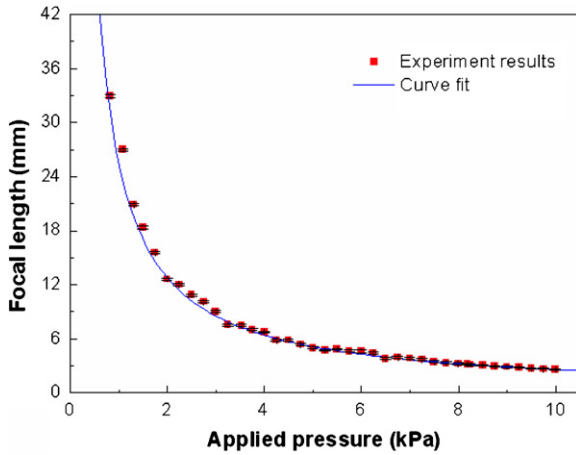


Figure 7. Focal length of the liquid-filled microlens as a function of applied pressure.

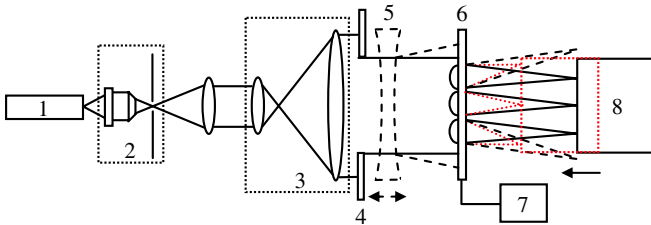


Figure 8. Schematic of the optical setup for proof-of-concept demonstration. (1) He–Ne laser, (2) spatial filter, (3) beam expander, (4) iris, (5) concave lens, (6) liquid microlens array, (7) pumping system, (8) CCD camera.

3.2. Proof-of-concept demonstration

Currently, a simple optical setup as shown in figure 8 is used to demonstrate one of the advantages, namely dynamic measurement range improvement, provided by this design concept for the Shack–Hartmann wavefront sensor. Light from a He–Ne laser is first collimated via a spatial filter component and a collimating lens. After propagating through a beam expander and an iris, the light is normally incident onto a CCD camera via a 6×5 liquid-filled microlens array placed before it. For this case, the CCD camera is placed onto a manual linear stage equipped with micrometers (NEWPORT), with which the position of the CCD-sensitive area can be adjusted along the optical axis with $1 \mu\text{m}$ sensitivity and 25 mm travel range to adapt to the focal plane variation of the microlens array during operation. Before the verification experiment, a calibration procedure is first performed, in which the central positions of all of the focal spots under illumination with collimated light are recorded separately at each working status (different focal lengths), using as the reference for the wavefront reconstruction under this condition. As a result, the effect of the possible on-axis position error induced by the linear stage on the reconstructed wavefront can be eliminated. During the proof-of-concept demonstration, the focal length of the liquid-filled microlens is initially tuned to 25.6 mm, and the resulted spots’ array on the CCD is shown in figure 9 (this is used as the reference for the following wavefront reconstruction). A concave lens is then inserted into an optical

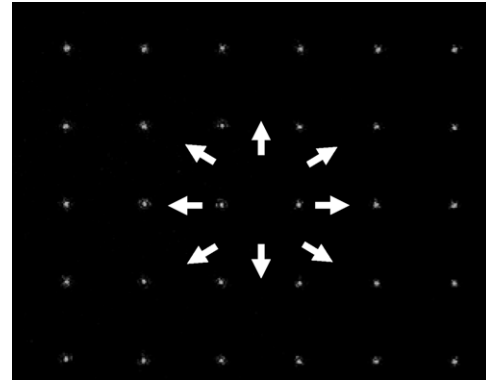


Figure 9. Spots’ array captured by the CCD when illuminating with a collimated light. Arrows denote the spots’ movement direction when the collimated light is changed into divergent light.

path to convert the light from collimation into divergence acting as a source of aberration. As a result, the spots will move accordingly. By adjusting the position of this concave lens along the optical axis, the resultant wavefront distortion on the sampling plane of the sensor can be changed causing the lateral movement of spots:

$$\Delta x(\Delta y)|_i \propto f \times S_{x(y)}|_i, \quad (3)$$

where $\Delta x|_i$ and $\Delta y|_i$ are the lateral movements of the focus of the i th microlens with f focal length along x - and y -directions, respectively, which are caused by the average wavefront slope $S_{x(y)}|_i$ within this subaperture.

In one extreme case, some spots will move out of the CCD-sensitive area (see figure 10(a)), therefore causing failure to the wavefront sensor. This is used to simulate the case that the aberration is beyond the measurement range of the wavefront sensor. When shortening the focal length to 7.88 mm and correspondingly placing the CCD at the new focal plane, the lateral movement of the spots will be decreased as described by equation (3) and all of the spots will be captured by the CCD again as shown in figure 10(b). By performing the same data treatment as that used in the standard Shack–Hartmann device [8, 9], the wavefront can be finally reconstructed as presented in figure 11. The result shows that there are three main components in the wavefront, including tilt in both x - and y -directions and defocusing. The wavefront tilt is caused by the misalignment between the central axis of the concave lens and the main optical axis of the system, constituting an additional aberration introduced by the concave lens. The relatively large defocusing aberration is mainly caused by the nature of the concave lens.

4. Discussion

4.1. Focal spot tracking

From the working theory of the Shack–Hartmann wavefront sensor, it is obvious that the exact position information of each focal spot in the array is most critical for wavefront reconstruction. In a situation where only one aspect of performance (e.g. large dynamic range or high sensitivity) is of concern, the main task is how to precisely detect

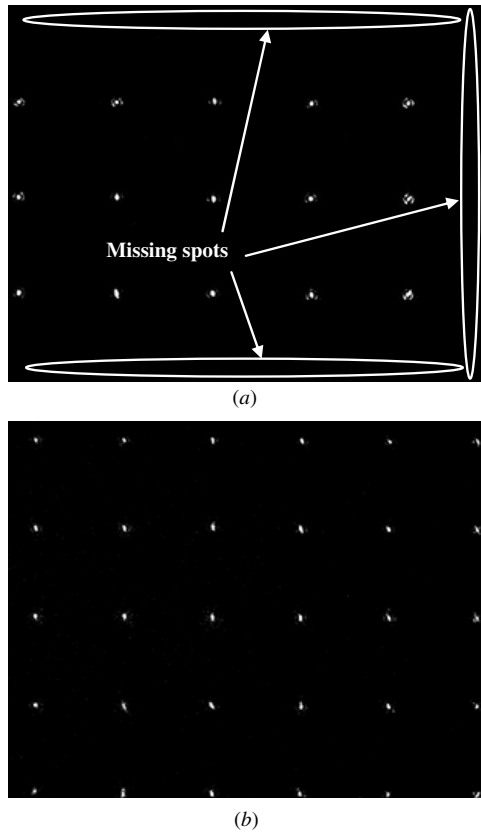


Figure 10. Spot array captured by the CCD under different working stages when an aberration is introduced. (a) Longer focal length and (b) shorter focal length.

the center position of the focal spot within each individual subaperture area on the CCD camera. Some research groups have focused their interest on this topic and some methods have been demonstrated successfully [25–28]. While for the cases that require both large dynamic range and high sensitivity, besides the same consideration on the centroid detection as mentioned above, a particular point tracking algorithm is also needed since the focal spots will move in accordance with the change of the microlens focal length. First, the microlens array is tuned to the shortest focal length (largest dynamic range) within the working range. At this moment, all the focal spots are located within their corresponding subaperture region. Therefore, the main task is to individually determine their center position. By comparing with the reference under this working condition, the lateral movements as well as the average wavefront slopes within each subaperture can be deduced. Then the microlens array is adjusted to the longest focal length (highest sensitivity). Due to the possibly large wavefront slope within some subaperture regions, in this case, their focal spots will enter into a neighboring subaperture area, thus confusing the wavefront reconstruction algorithm. This problem is difficult to solve in the conventional Shack–Hartmann wavefront sensor equipped with a solid microlens array. But as for our configuration, this will not be a problem anymore. It is because we have already obtained preliminary information about the wavefront under test from the previous experiment, namely using the shortest focal length of the

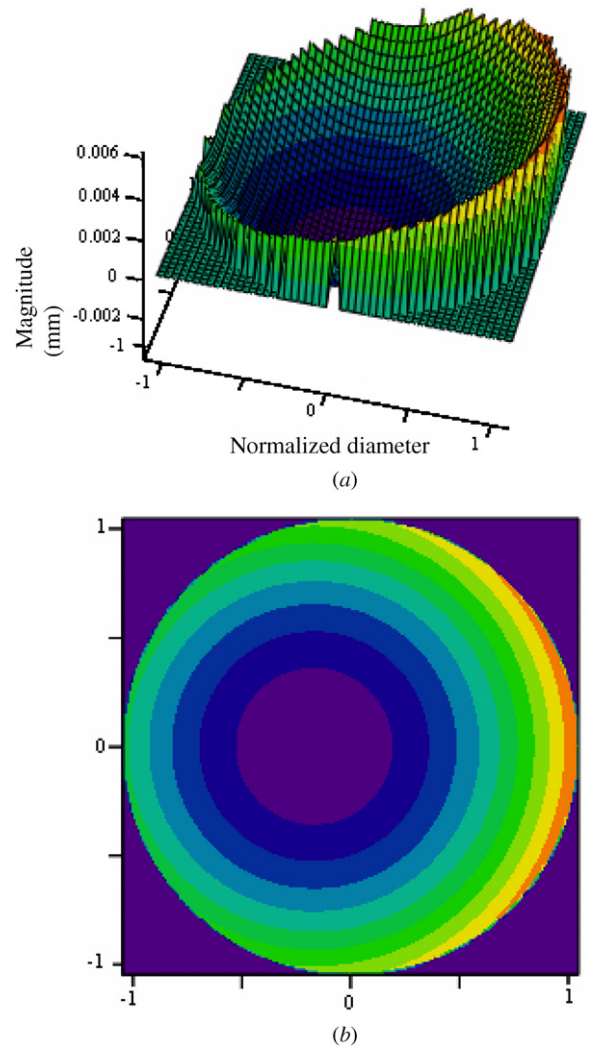


Figure 11. Reconstructed wavefront. (a) 3D profile and (b) 2D contour.

array. From equation (3), it is obvious that the resultant lateral movement of the focal spot is proportional to the focal length. As a result, we can first predict the center position of each focal spot by using information about the average wavefront slope obtained in the previous measurement and then perform a local search near the estimated spot center, taking into account the possible positioning error introduced by the movement of the CCD (as mentioned in section 3.2). The centroid positions of the focal spots as well as the wavefront can be finally detected. This is illustrated in figure 12.

4.2. Application perspective

The new concept of applying the liquid microlens array with tunable focal length capability into the Shack–Hartmann wavefront sensor will bring distinct advantages to some applications, especially for adaptive optics. Figure 13 is the concept demonstration in an AO system. The light is first incident onto the deformable mirror. The reflected light will then be divided into two parts by a beamsplitter: one is directly captured by a CCD camera and the other one is incident

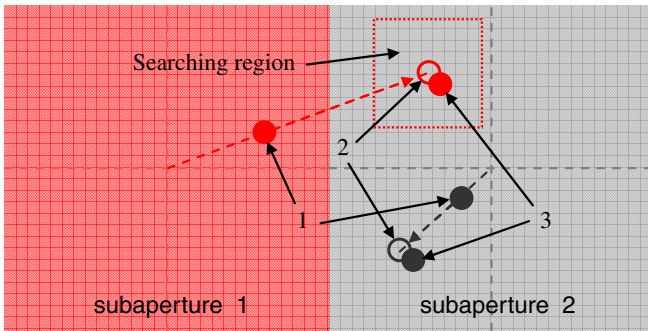


Figure 12. Schematic of the focal point tracking algorithm (The grey (red online) spot stands for the focal spot created by the microlens belonging to subaperture 1, while the light gray spot corresponds to the focal spot from the subaperture 2 assigned microlens.) (1) Focal spot at the shortest focal length (measured), (2) focal spot at the longest focal length (estimated), (3) focal spot at the longest focal length (real).

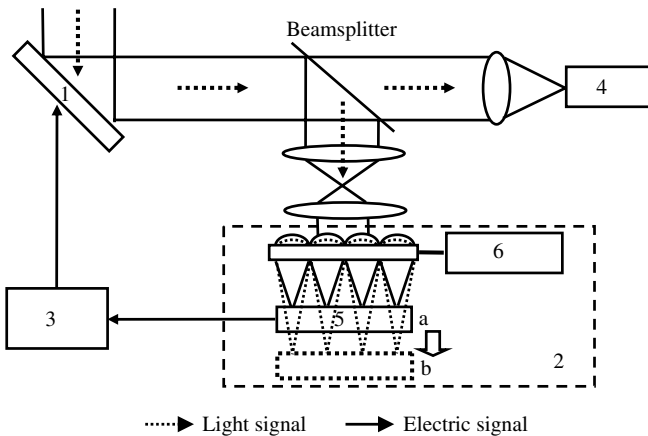


Figure 13. Schematic of the AO system. (1) Deformable mirror, (2) wavefront sensor, (3) controller, (4), (5) CCD camera, (6) liquid pressure control system; a and b are the focal planes of the microlens with shorter and longer focal lengths, respectively.

onto the wavefront sensor via a converted telescope (adapting the beam width to the wavefront sensor). The shorter focal length is initially used. As a result, large wavefront distortion information can be obtained followed by being transferred to the controller. Through proper data treatment, the resultant control signal is then sent to the deformable mirror to perform coarse correction with the use of a particular closed-loop control algorithm. Then the microlens is tuned into a longer focal length status. With the same work procedure, the finer correction can be finally achieved. Therefore, the AO system can highly benefit from the use of liquid-filled microlens with the capability of a large dynamic correction range together with high resolution.

In our design, the CCD camera needs to be moved accordingly during device operation, in order to adapt to the change of the focal length as well as the focal plane of the microlens in the array. Unlike the case of proof-of-concept demonstration, in real applications a computer-controlled mechanical component, for example a linear motor stage, is required to obtain fast and precise positioning with high repeatability (such as XMS series linear motor stages from

NEWPORT). Despite the good specifications provided by the motor stage, the AO systems incorporating our device are more appropriate for compensating the aberration with relatively slow time-dependent variation (such as several Hertz) and static aberration. For example, in vision science, an adaptive optics system operating with a closed-loop bandwidth of 1–2 Hz is adequate to capture the most important temporal changes in the fixating eye [29, 30] whilst in high power solid-state laser application, the aberration, namely the thermal lens effect, is directly dependent on the pump power [31, 32]. Once the pump power is fixed, the resulted focal length of the thermal lens will be determined accordingly [33, 34]; therefore, in this case, the aberration can be approximately treated as a static one. By constructing intracavity adaptive optics, the laser output with high beam quality can be chosen to work within a large power range [35, 36].

5. Conclusion

In conclusion, a unique configuration for the Shark–Hartmann wavefront sensor is presented. The commonly used microlens array with fixed focal length is replaced by a liquid-filled microlens array integrated with a microfluidic network. The focal length of this type of microlens can be easily adjusted by only changing the pumping pressure. During operation, the longer focal length is used to provide the device with a capability of detecting wavefront with high sensitivity, while a performance of a large dynamic measurement range can be realized in the shorter focal length working status. A 6×5 liquid-filled microlens array is used for qualitative demonstration of this configuration concept. A concave lens is used to introduce a defocusing item into the light under test. In the case of longer focal length, the aberrated wavefront can cause some sampling spots moving out of the CCD-sensitive area. This is used to simulate the situation that the aberration is beyond the measurement range of the sensor. By shortening the focal length, all of these missing spots can be again captured by the CCD, and the wavefront is then successfully reconstructed as predicted from theoretical analysis. With this design concept, a versatile Shack–Hartmann wavefront sensor can be realized. Its working performance can be conveniently chosen from a large dynamic measurement range preferred to high sensitivity meant to meet the requirements of different applications. At the same time, by using a particular operation procedure and spot tracking algorithm, both large dynamic measurement range and high sensitivity performance can be achieved simultaneously in one device. This device configuration will also bring advantages to some applications especially for AO systems requiring low closed-loop operation bandwidth, in which the coarse correction can be performed under the shorter focal length status, while the longer focal length can be used for fine compensation.

Acknowledgment

Financial support by the Ministry of Education (MOE) Singapore AcRF Tier 1 funding under grant nos R-265-000-235-112 and R-265-000-211-112/133 is gratefully acknowledged.

References

- [1] Malacara D and Thompson B J 2001 *Handbook of Optical Engineering* (New York: Dekker)
- [2] Samarkin V, Zavalova V, Alexandrov A, Roukossouev A and Kudryashov A 2003 Adaptive optics for high power laser beam shaping *Proc. IEEE Conf. on Lasers and Electro-Optics Europe (New York, USA)* p 107
- [3] Chanan G, Troy M, Dekens F, Michaels S, Nelson J, Mast T and Kirkman D 1998 Phasing the mirror segments of the Keck telescopes: the broadband phasing algorithm *Appl. Opt.* **37** 140–55
- [4] Salmon T O, Thibos L N and Bradley A 1998 Comparison of the eye's wave-front aberration measured psychophysically and with the Shack–Hartmann wave-front sensor *J. Opt. Soc. Am. A* **15** 2457–65
- [5] Liang J, Grimm B, Goelz S and Bille J 1994 Objective measurement of wave aberrations of the human eye with use of a Hartmann–Shack wave-front sensor *J. Opt. Soc. Am. A* **11** 1949–57
- [6] Manzanera S, Canovas C, Prieto P M and Artal P 2008 A wavelength tunable wavefront sensor for the human eye *Opt. Express* **16** 7748–55
- [7] Platt B C and Shack R 2001 History and principles of Shack–Hartmann wave-front sensing *J. Refract. Surg.* **17** 573–7
- [8] Wyant J C 1999 *Zernike Polynomial* (University of Arizona, AZ: Optical Science Center)
- [9] Zhu L, Sun P C, Bartsch D U, Freeman W R and Fainman Y 1999 Adaptive control of a micromachined continuous-membrane deformable mirror for aberration compensation *Appl. Opt.* **38** 168–76
- [10] Lee J, Shack R V and Descour M R 2005 Sorting method to extend the dynamic range of the Shack–Hartmann wave-front sensor *Appl. Opt.* **44** 4838–45
- [11] Roggemann M C and Schulz T J 1998 Algorithm to increase the largest aberrations that can be reconstructed from Hartmann sensor measurements *Appl. Opt.* **37** 4321–9
- [12] Pfund J, Lindlein N and Schwider J 1998 Dynamic range expansion of a Shack–Hartmann sensor by use of a modified unwrapping algorithm *Opt. Lett.* **23** 995–7
- [13] Seifert L, Tiziani H J and Osten W 2005 Wavefront reconstruction with the adaptive Shack–Hartmann sensor *Opt. Commun.* **245** 255–69
- [14] Choo H and Muller R S 2006 Addressable microlens array to improve dynamic range of Shack–Hartmann sensors *J. Microelectromech. Syst.* **15** 1555–67
- [15] Yoon G, Pantanelli S and Nagy L J 2006 Large-dynamic-range Shack–Hartmann wavefront sensor for highly aberrated eyes *J. Biomed. Opt.* **11** 030502-1–030502-3
- [16] Zhang D Y, Justis N and Lo Y H 2004 Fluidic adaptive lens of transformable lens type *Appl. Phys. Lett.* **84** 4194–6
- [17] Agarwal M I, Gunasekaran R A, Coane P and Varahramyan K 2004 Polymer-based variable focal length microlens system *J. Micromech. Microeng.* **14** 1665–73
- [18] Chen J, Wang W, Fang J and Varahramyan K 2004 Variable-focusing microlens with microfluidic chip *J. Micromech. Microeng.* **14** 675–80
- [19] Yang H, Yang C Y and Yeh M S 2007 Miniaturized variable-focus lens fabrication using liquid filling technique *Microsyst. Technol.* **14** 1067–72
- [20] Zhang D Y, Justis N, Lien V, Berdichevsky Y and Lo Y H 2004 High-performance fluidic adaptive lenses *Appl. Opt.* **43** 783–7
- [21] Yu H B, Zhou G Y, Chau F S and Lee F W 2008 Optofluidic variable aperture *Opt. Lett.* **33** 548–50
- [22] Zhang D Y, Lien V, Berdichevsky Y, Choi J and Lo Y H 2003 Fluidic adaptive lens with high focal length tenability *Appl. Phys. Lett.* **82** 3171–3
- [23] Zhang D Y, Justis N and Lo Y H 2004 Integrated fluidic adaptive zoom lens *Opt. Lett.* **15** 2855–7
- [24] Chronis N, Liu G L, Jeong K H and Lee L P 2003 Tunable liquid-filled microlens array integrated with microfluidic network *Opt. Express* **11** 2370–8
- [25] Thomas S 2004 Optimized centroid computing in a Shack–Hartmann sensor *Proc. SPIE* **5490** 1238–46
- [26] Jiang Z L, Gong S S and Dai Y 2004 Monte-Carlo analysis of centroid detected accuracy for wavefront sensor *Opt. Laser Technol.* **37** 541–6
- [27] Baker K L and Moallem M M 2007 Iteratively weighted centroiding for Shack–Hartmann wave-front sensors *Opt. Express* **15** 5147–59
- [28] Baik S H, Park S K, Kim C J and Cha B 2007 A center detection algorithm for Shack–Hartmann wavefront sensor *Opt. Laser Technol.* **39** 262–7
- [29] Jason P, Hope M Q, Julianna E L, Karen T and Abdul A 2006 *Adaptive Optics for Vision Science: Principles, Practices, Design, and Applications* (New York: Wiley)
- [30] Hofer H, Artal P, Singer B, Aragón J L and Williams D R 2001 Dynamics of the eye's wave aberration *J. Opt. Soc. Am. A* **18** 497–506
- [31] Rüdiger P 2008 *Encyclopedia of Laser Physics and Technology* (New York: Wiley)
- [32] Wittrock U 2005 Adaptive optics for industry and medicine *Proc. 4th Int. Workshop* (Berlin: Springer)
- [33] Jacinto C, Catunda T, Jaque D, Bausá L E and García-Solé J 2008 Thermal lens and heat generation of Nd:YAG lasers operating at 1.064 and 1.34 μm *Opt. Express* **16** 6317–23
- [34] Hoos F, Li S, Meyrath T P, Braun B and Giessen H 2008 Thermal lensing in an end-pumped Yb:KGW slab laser with high power single emitter diodes *Opt. Express* **16** 6041–9
- [35] Yang P, Liu Y, Yang W, Ao M W, Hu S J, Xu B and Jiang W H 2007 Adaptive mode optimization of a continuous-wave solid-state laser using an intracavity piezoelectric deformable mirror *Opt. Commun.* **278** 377–81
- [36] Yang P, Ao M W, Liu Y, Xu B and Jiang W H 2007 Intracavity transverse modes controlled by a genetic algorithm based on Zernike mode coefficients *Opt. Express* **15** 17051–62